Diffusion MRI in Peripheral Nerves: Optimized *b* Values and the Role of Non-Gaussian Diffusion

Olivia Foesleitner, MD, PhD • *Alba Sulaj, MD* • *Volker Sturm, PhD* • *Moritz Kronlage, MD* • *Tim Godel, MD* • *Fabian Preisner, MD* • *Peter Paul Nawroth, MD* • *Martin Bendszus, MD* • *Sabine Heiland, PhD* • *Daniel Schwarz, MD*

From the Department of Neuroradiology (O.F., V.S., M.K., T.G., F.P., M.B., S.H., D.S.) and Department of Internal Medicine I and Clinical Chemistry (A.S., P.P.N.), Heidelberg University Hospital, Im Neuenheimer Feld 400, 69120 Heidelberg, Germany; German Center for Diabetes Research (DZD), Helmholtz Center Munich, Neuherberg, Germany (P.P.N.); Joint Division Molecular Metabolic Control, German Cancer Research Center (DKFZ), Heidelberg Center for Molecular Biology (ZMBH), Heidelberg, Germany (P.P.N.); and Institute for Diabetes and Cancer IDC Helmholtz Center Munich and Joint Heidelberg-IDC Translational Diabetes Program, Neuherberg, Germany (P.P.N.). Received January 4, 2021; revision requested February 8; revision received July 23; accepted August 4. **Address correspondence to** D.S. (e-mail: *daniel.schwarz@med.uni-heidelberg.de*).

Background: Diffusion-weighted imaging (DWI) provides specific in vivo information about tissue microstructure, which is increasingly recognized for various applications outside the central nervous system. However, standard sequence parameters are commonly adopted from optimized central nervous system protocols, thus potentially neglecting differences in tissue-specific diffusional behavior.

Purpose: To characterize the optimal tissue-specific diffusion imaging weighting scheme over the *b* domain in peripheral nerves under physiologic and pathologic conditions.

Materials and Methods: In this prospective cross-sectional study, 3-T MR neurography of the sciatic nerve was performed in healthy volunteers (*n* = 16) and participants with type 2 diabetes (*n* = 12). For DWI, 16 *b* values in the range of 0–1500 sec/mm² were acquired in axial and radial diffusion directions of the nerve. With a region of interest–based approach, diffusion-weighted signal behavior as a function of *b* was estimated using standard monoexponential, biexponential, and kurtosis fitting. Goodness of fit was assessed to determine the optimal *b* value for two-point DWI/diffusion tensor imaging (DTI).

Results: Non-Gaussian diffusional behavior was observed beyond *b* values of 600 sec/mm² in the axial and 800 sec/mm² in the radial diffusion direction in both participants with diabetes and healthy volunteers. Accordingly, the biexponential and kurtosis models achieved a better curve fit compared with the standard monoexponential model (Akaike information criterion >99.9% in all models), but the kurtosis model was preferred in the majority of cases. Significant differences between healthy volunteers and participants with diabetes were found in the kurtosis-derived parameters D_k and *K*. The results suggest an upper bound *b* value of approximately 700 sec/mm² for optimal standard DWI/DTI in peripheral nerve applications.

Conclusion: In MR neurography, an ideal standard diffusion-weighted imaging/diffusion tensor imaging protocol with *b* = 700 sec/mm² is suggested. This is substantially lower than in the central nervous system due to early-occurring non-Gaussian diffusion behavior and emphasizes the need for tissue-specific *b* value optimization. Including higher *b* values, kurtosis-derived parameters may represent promising novel imaging markers of peripheral nerve disease.

©RSNA, 2021

Online supplemental material is available for this article.

MR diffusion-weighted imaging (DWI) comprises a number of popular techniques with a wide range of clinical applications based on tissue-specific Brownian molecular motion, including diffusion tensor imaging (DTI) as an important extension of standard DWI to provide directional information of restricted water diffusion (1). These techniques have primarily been optimized in the central nervous system, providing in vivo information about neuronal fiber integrity and tissue architecture (2).

While DWI/DTI is increasingly recognized and applied outside the central nervous system (3–5), certain technical aspects, including the selection of diffusion weighting (ie, *b* value), have largely been empirically adapted from investigations within the central nervous system (6,7). Additionally, in MR neurography, diffusion-based techniques have become popular as a functional marker providing additional diagnostic value compared with conventional T2-weighted MR neurography (8–12). Interestingly, to our knowledge, there is still no consensus with regard to optimal diffusion weighting in peripheral nerve DWI/DTI (13).

Correct *b* value selection, however, critically determines the accuracy and reliability of quantitative diffusion parameters, as the signal-to-noise ratio (SNR) decreases drastically with increasing *b* value.

Furthermore, non-Gaussian diffusion becomes increasingly important at higher *b* values, which is believed to reflect tissue microstructure. Thus, the measured signal decay

Abbreviations

DTI = diffusion tensor imaging, DWI = diffusion-weighted imaging, ROI = region of interest, SI = signal intensity, SNR = signal-to-noise ratio

Summary

Due to non-Gaussian diffusion behavior at low b values, the optimal b value for reliable diffusion-weighted imaging/diffusion tensor imaging within peripheral nerves should be set at approximately 700 sec/mm^2, highlighting the need for tissue-specific b value selection.

Key Results

- In a prospective study with 28 participants, relevant non-Gaussian diffusion behavior was observed at low b values within peripheral nerves.
- The optimal b value for standard two-point diffusion-weighted and diffusion tensor imaging could be determined between 600 and 800 sec/mm^2, substantially lower than in the central nervous system; an ideal diffusion protocol with $b = 700$ sec/mm^2 is therefore suggested for clinical nerve imaging.
- The kurtosis model achieves excellent signal fitting at higher b values and may provide promising novel biologic markers for peripheral neuropathies.

is poorly approximated with standard monoexponential fitting (14,15). To account for this effect, extended models like the kurtosis (16,17) or biexponential models (18) are usually adopted for a more accurate fit. In the brain, the common standard for the monoexponential model is a critical b value of approximately 1000 sec/mm^2, and significant non-Gaussian diffusion phenomena are expected beyond this value (19). In peripheral nervous tissue, in contrast, such a critical b value remains unknown.

Therefore, the aim of this study was to characterize the physiologic behavior of the diffusion-weighted signal as a function of b in the sciatic nerve of healthy volunteers and under pathologic conditions to establish the optimal b value for diagnostic diffusion imaging. In a second step, we compared the quality of signal fitting according to the kurtosis and biexponential models with the standard monoexponential fit.

Materials and Methods

Study Design and Participants

This prospective cross-sectional study was approved by the institutional ethics committee (S-398/2012 and S-682/2016) and performed in accordance with the 2013 revision of the Declaration of Helsinki. Written informed consent was obtained from all participants. Sixteen healthy volunteers without preexisting disease were recruited by means of public announcement (eight women; median age, 23 years [range, 21–31 years]). Additionally, 12 patients with type 2 diabetes and varying degrees of diabetic peripheral neuropathy were enrolled (two women; median age, 69 years; range, 54–73 years) (Table 1). Patients with confounding preexisting conditions other than diabetes possibly causing peripheral neuropathy (eg, nerve root–specific symptoms or a history of root impingement) were excluded.

MRI Acquisition and Analysis

All MR neurography examinations were performed with use of a 3-T scanner (Magnetom Prisma^{fit}, Siemens Healthineers) between August 2019 and March 2020. A 15-channel transmit-receive phased-array radiofrequency coil (Siemens Healthineers) was used. DWI scans were acquired in the fixed read (radial) and section (axial) directions of the diffusion-sensitizing gradients with use of a single spin-echo multi-b-value preparation comprising 16 b values between 0 and 1500 sec/mm^2, approximately matching the radial and axial diffusion direction of the nerve. The b values were changed, keeping pulse width constant, while only the amplitude was varied. Further sequence details are summarized in Table 2.

In healthy volunteers, the tibial part of the sciatic nerve was first identified on four representative sections at axial T2-weighted imaging. Subsequently, the regions of interest (ROIs) in the nerve were manually segmented on the B0 images of the corresponding diffusion-weighted sequences, and mean signal intensity (SI) values were extracted using

Table 1: Data and Severity Scores for Participants with Diabetes

Participant No.	Age (y)	Sex	Disease duration (y)	BMI (kg/m²)	HbA1c (%)	Creatinine Level (mg/dL)	eGFR (mL/min)	NDS	NSS
1	63	F	30	24.4	8.1	0.57	99.0	0	0
2	69	M	7	23.0	6.5	0.7	96.3	4	8
3	69	M	29	30.7	7.7	0.73	94.6	5	9
4	62	M	10	31.3	6.5	0.77	97.3	2	6
5	68	M	20	29.2	8.8	0.82	90.8	4	6
6	72	M	1.5	28.2	6.0	0.92	82.8	8	8
7	73	M	1.5	23.5	6.1	1.35	51.7	4	7
8	54	M	20	29.3	7.4	0.57	116.4	0	7
9	69	M	3	33.6	6.8	1.45	49.1	4	7
10	73	F	33	29.4	9.2	0.59	91.2	5	9
11	68	M	6	34.2	9.6	0.99	77.9	2	6
12	68	M	6	29.1	7.4	0.72	96.5	1	0

Note.—BMI = body mass index, eGFR = estimated glomerular filtration rate, HbA1c = hemoglobin A1c, NDS = neuropathy disability score, NSS = neuropathy symptom score.

OsiriX (Pixmeo). Background noise for each b value was measured within an ROI of 400 mm².

In participants with diabetes, two readers (O.F. and D.S., with 2 and 8 years of experience, respectively, in MR neurography) first independently assessed morphologic features of the nerve on each of all 35 sections of the axial T2-weighted MR neurography sequence as normal, pathologic, mixed (ie, normal and pathologic fascicles on the same section), or inconclusive (20), with high interrater reliability (Cohen κ of 0.92). From all matching section pairs, one normal-appearing (hereafter, T2-normal) and one pathologic (here-after, T2-pathologic) nerve region per patient was identified in a concluding consensus reading. ROI analysis of these regions was subsequently performed as in the controls.

Data Processing
SI decay within identified ROI of the nerve as a function of b was fitted over the entire range of b values by using a monoexponential model (Eq [1]) assuming Gaussian diffusivity and by using a biexponential model (Eq [2]) as well as the kurtosis model (Eq [3]) to account for possible non-Gaussian diffusion behavior (16):

$$S = S_0 \times e^{-b \times D}, \tag{1}$$

where D represents the apparent diffusion coefficient (10^{-3} mm²/sec);

$$S = S_0 \times \left(f e^{(-b \times D_f)} + (1 - f) e^{(-b \times D_i)} \right), \tag{2}$$

where D_f and Ds represent the fast and slow diffusion coefficients (10^{-3} mm²/sec), respectively, and f represents the fraction of fast diffusion; and

$$S = S_0 \times e^{\left(-b \times D_k + \frac{1}{6} \times b^2 \times D_k^2 \times K \right)}, \tag{3}$$

where D_k represents the kurtosis-derived apparent diffusion coefficient (10^{-3} mm²/sec) and K is an additional, unitless parameter. Parameter maps of D_k and K were generated using a custom-written Matlab routine (R2015a, MathWorks).

Fitting models were compared using the Akaike information criterion corrected for small sample sizes, or AICc, as implemented in Prism version 8 (GraphPad Software). To assess the goodness of fit of the model implementations, the relative deviation from mean SI values was calculated and plotted as a function of b.

To test for group differences in K and D_k between healthy volunteers and participants with diabetes, the nonparametric Kruskal-Wallis test and Dunn correction were used. For T2-normal versus T2-pathologic nerve regions in participants with diabetes, the nonparametric Wilcoxon signed-rank test was employed. $P < .05$ was considered indicative of statistically significant difference.

Results

Diffusion-weighted Signal in Healthy Volunteers and Participants with Diabetes
We first measured the signal decay of the sciatic nerve and the background noise level along the axial and radial diffusional

Table 2: Sequence Parameters

Parameter	Diffusion-weighted Imaging	T2-weighted Sequence
Repetition time (msec)	4300	6969
Echo time (msec)	93	54
Field of view (mm)	160 × 160	140 × 140
Matrix	120 × 120	512 × 358
Section thickness (mm)	4.0	3.5
No. of sections	15	35
Section gap (mm)	0.4	0.35
No. of averages	4	3
Parallel imaging	GRAPPA	GRAPPA
Acceleration factor	2	2
No. of reference lines	38	32
Acquisition time per slab (min)	4:37	5:29
Fat saturation	SPAIR	Spectral fat saturation
b Value (sec/mm²)	0, 50, 100, 150, 200, 250, 300, 350, 400, 450, 500, 600, 800, 1000, 1200, 1500	NA
Pulse width (δ)	Constant, 21.0 msec	NA
Delta (Δ)	Constant, 62.9 msec	NA

Note.—GRAPPA = generalized autocalibrating partial parallel acquisition, NA = not applicable, SPAIR = spectral adiabatic inversion recovery.

domain over a wide range of b values in healthy volunteers (Fig 1). Within the entire range of b values, mean SI in the ROI of the nerve remained several times above noise level in both diffusional domains at a consistently high SNR (Table E1 [online]), so a reliable signal recording of nerve tissue can be assumed up to b of 1500 sec/mm². Interestingly, the observed SI decay was not found to be monoexponential but flattened out well before b of 1000 sec/mm², suggesting non-Gaussian diffusional effects at relatively low b values (Fig 1B). Comparison of curve fitting between the monoexponential (Eq [1]), biexponential (Eq [2]), and kurtosis models (Eq [3]) thus revealed a significantly better approximation of the latter two in both diffusion directions, expressed as greater than 99.9% model probability according to the corrected Akaike information criterion for each of these extended models (Fig 2A).

We next asked whether such a signal behavior was also present under pathologic conditions. Therefore, a sample of participants with type 2 diabetes was additionally studied. As in healthy volunteers, an ROI-based analysis was performed, including one T2-normal and one T2-pathologic nerve region. Again, the SI decay departed from a monoexponential function (Figs 2B, 3, E1 [online]), likewise suggesting non-Gaussian diffusion behavior. The biexponential and kurtosis models both achieved a better curve fit, with over 99.9% model preference compared with monoexponential fitting according to the Akaike information criterion corrected for small sample sizes (Figs 2B, E2 [online]).
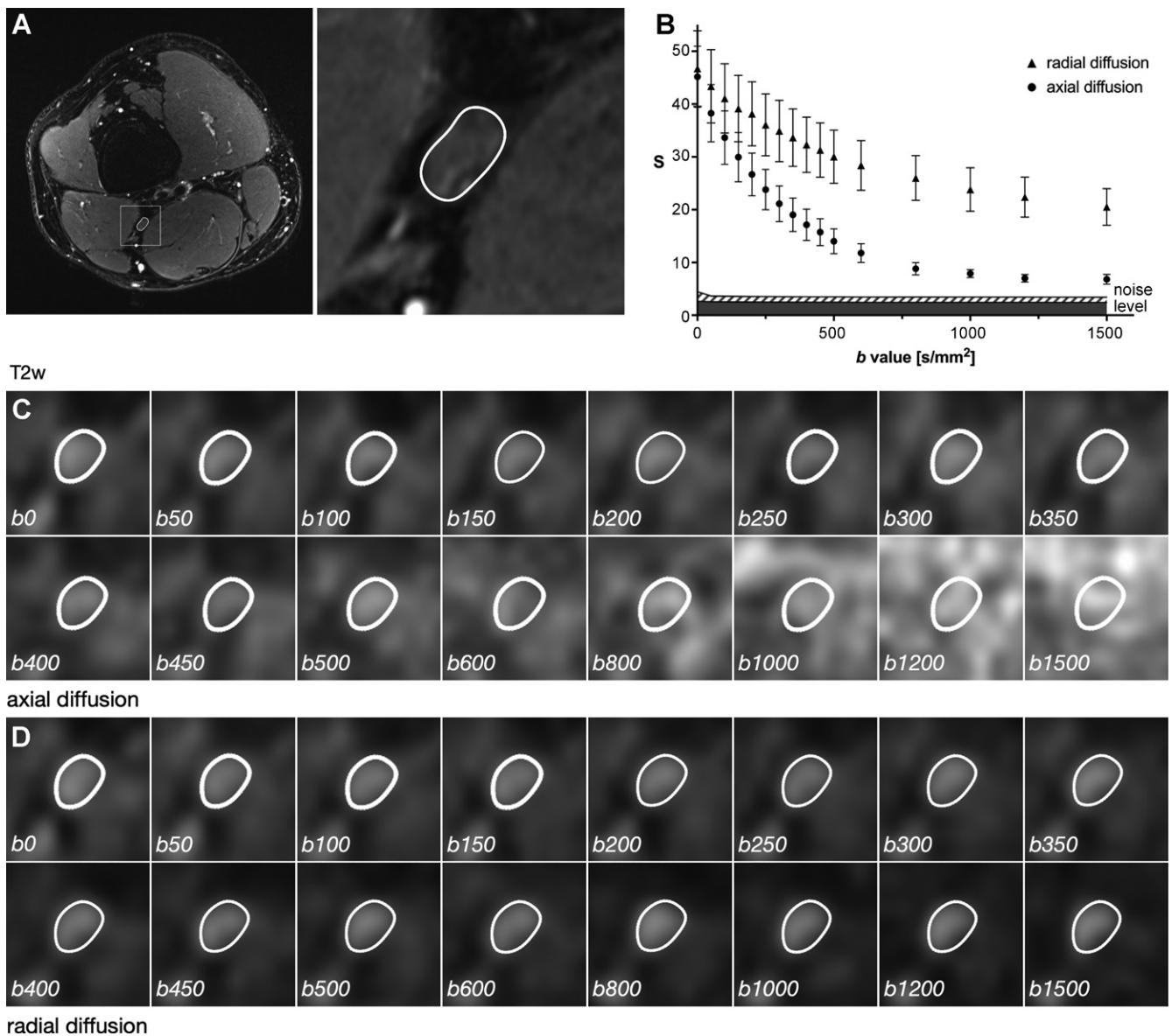
Figure 1: Diffusion-weighted imaging signal decay in healthy volunteers. **(A)** T2-weighted (T2w) images and series of diffusion-weighted images at 16 measured *b* values in **(C)** axial and **(D)** radial directions in a representative healthy volunteer. Segmentation of the tibial nerve is indicated by a white contour. **(B)** Inserted graph depicts the diffusion-weighted signal (S) measured within the region of interest (ROI) of the nerve as a function of *b* in healthy volunteers (arbitrary units). Error bars represent 95% CIs. Noise levels within a standardized region of interest are also shown with 95% CIs (light and dark gray shaded areas). Signal in ROI of the nerve remains well above noise level. In **C** and **D**, the window level of each magnified image is set to a linear gray scale from 0 to twice the magnitude signal of each ROI of the nerve.

Threshold *b* Value Suggestions for Standard DWI/DTI

Since the usual postprocessing of DWI/DTI uses only two *b* values and assumes a monoexponential signal decay, the results presented would be crucial for correct selection of the upper *b* value. Therefore, we aimed to establish an optimal threshold range of *b* values that would grant strong diffusional weighting and low systematic errors.

To compare the goodness of fit of the different models considered, we calculated the relative deviation of the model fits from the measured normalized SI and plotted them as a function of *b* (Fig 4). Assuming a tolerable deviation of approximately 10%, the monoexponential model obviously does not yield useful fitting results beyond a threshold range of *b* of 600–800 sec/mm². Interestingly, there appears to be a direction-dependent

component involved with a lower *b* threshold in the axial diffusion direction (*b* = approximately 600 sec/mm²) and a higher threshold in the radial diffusion direction (*b* = approximately 800 sec/mm²).

Kurtosis Parameters D_k and *K*

While both of the extended approaches (ie, the biexponential and kurtosis models) provide an excellent fit to the measured data under physiologic and pathologic conditions (all $R^2 >$ 0.98), we next addressed the question of which one was superior. When the Akaike information criterion corrected for small sample sizes was used, preference was given to the kurtosis model in five of six conditions (Table E2 [online]). Assuming this to represent the most appropriate and simplest model, the
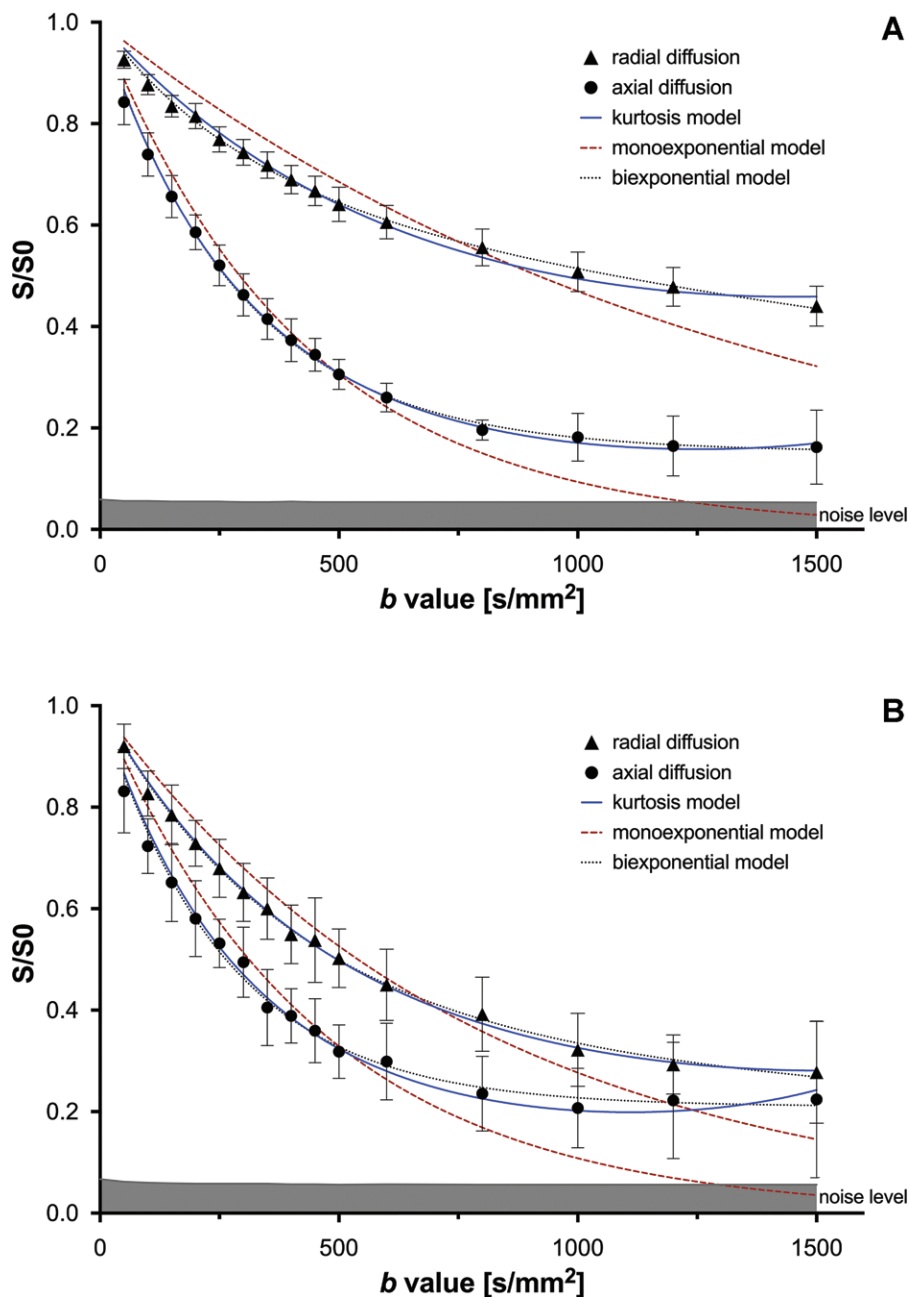
Figure 2: Diffusion models in healthy volunteers and participants with diabetes. Curve fitting of the diffusion-weighted signal as a function of *b* in **(A)** healthy volunteers and **(B)** participants with diabetes in axial and radial diffusion directions. Error bars are 95% CIs. Up to *b* of 1500 sec/mm², the kurtosis model (solid blue line) and biexponential model (dotted black line) achieved a significantly better approximation of the diffusion-weighted signal curve than the standard monoexponential model (dashed red line) in both diffusional domains.

kurtosis-specific parameters of K and D_k were further investigated. In healthy volunteers, the values of D_k were 2.92×10^{-3} mm²/sec for axial and 1.08×10^{-3} mm²/sec for radial diffusion, respectively, and K yielded values of 0.75 for the axial and 1.95 for the radial diffusion.

Compared with controls, lower values of K were found in T2-normal and T2-pathologic diabetic nerve regions in the radial diffusion direction ($P = .022$ and $P < .001$, respectively) (Fig 5A). In the axial diffusional domain, K was lower in controls than in T2-normal diabetic nerve regions ($P = .021$). Higher

values of D_k were found in both T2-normal and T2-pathologic nerve regions of participants with diabetes compared with controls in the radial diffusional direction only ($P = .002$ and $P = .004$, respectively) (Fig 5B). Figure 6 shows a direct comparison of kurtosis-mapping results between a healthy volunteer and a participant with diabetes.

Discussion

In this study, we rigorously investigated optimal *b* values for diffusion imaging of peripheral nervous tissue under physi-
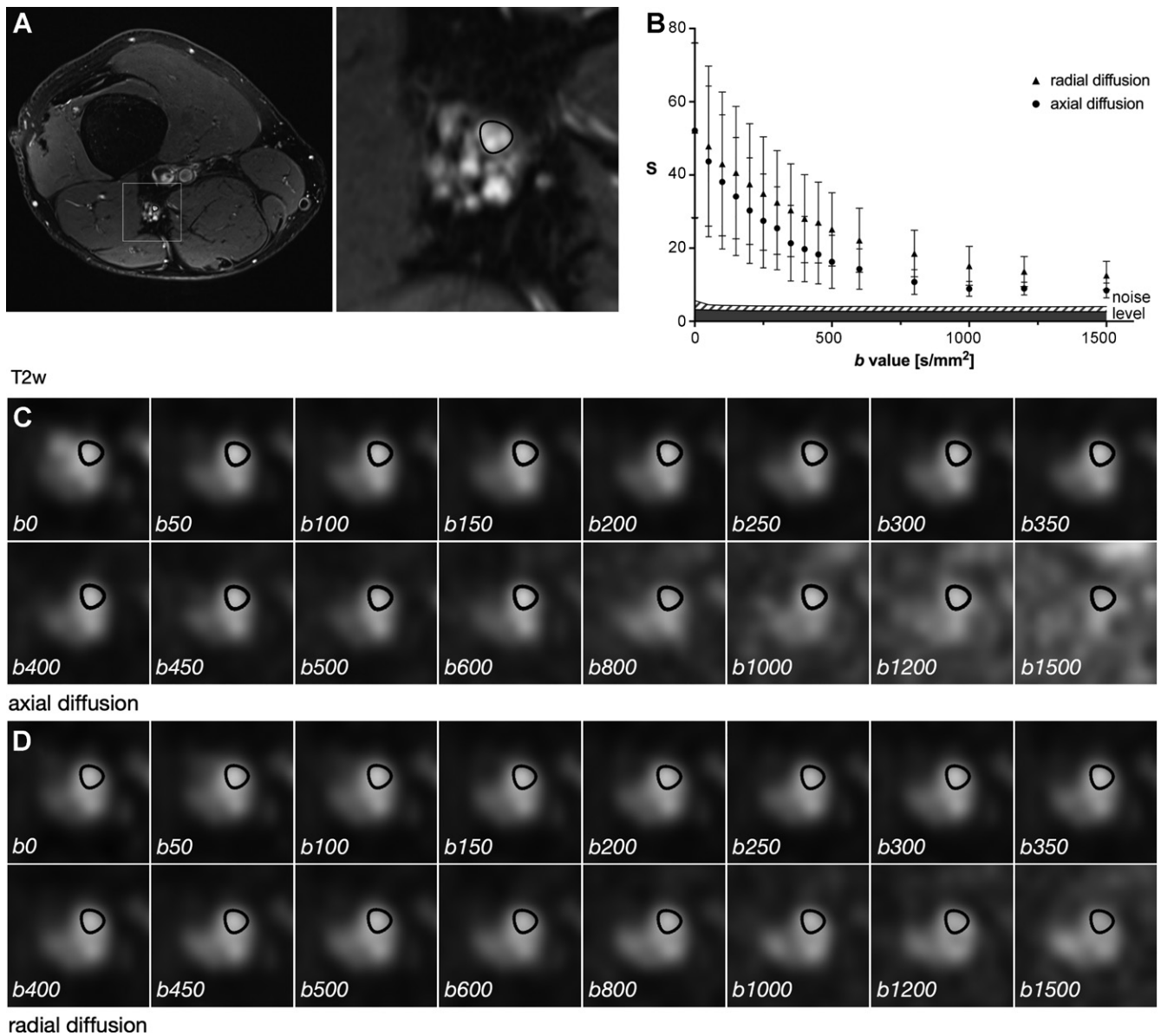
Figure 3: Diffusion-weighted imaging nerve lesions in participants with diabetes. **(A)** T2-weighted (T2w) images and series of diffusion-weighted images at 16 *b* values acquired in **(C)** axial and **(D)** radial diffusional domains in the T2-pathologic nerve part of a representative patient with diabetes (participant 2 in Table 1). Segmentation of the tibial nerve is indicated by a black contour. **(B)** Inserted graph depicts the diffusion-weighted signal (S) measured within the region of interest (ROI) of the nerve as a function of *b* in participants with diabetes (arbitrary units). Error bars represent 95% CIs. Noise levels within a standardized region of interest are also shown with 95% CIs (light and dark gray shaded areas). Signal in ROI of the nerve remains well above noise level in both radial and axial directions over the entire range of *b* values. In **C** and **D**, the window level of each magnified image is set to a linear gray scale from 0 to twice the magnitude signal of each ROI of the nerve.

ologic and pathologic conditions. In a homogeneous environment, molecular diffusivity is unrestricted and Gaussian, following a monoexponential signal decay over the *b* domain. Herein, however, we show non-Gaussian diffusional behavior occurring at low *b* values of less than 1000 sec/mm² in both healthy volunteers and participants with diabetes and identify an optimal upper *b* value of approximately 700 sec/mm². This seems even more remarkable because, commonly, such effects are only expected to be relevant for *b* values greater than 1000–1500 sec/mm² (14,15,19,21). Importantly, our observations occur within the clinically applied range of *b* for standard diffusion-weighted imaging/diffusion tensor imaging in MR

neurography, with current recommendations ranging up to 1000–1400 sec/mm² (22,23).

We hypothesize this could be due to tissue-specific differences between the central nervous system and peripheral nervous system, but the influence of complex noise may also be a confounding factor; indeed, SI as a function of *b* does not approach 0 but rather the noise floor for high *b* values even under unrestricted conditions, creating a similar appearance to non-Gaussian diffusion. This, however, is typically seen at a very low SNR. As our SNR was greater than 7 even for the highest *b* values, this does not constitute a confounding factor in our study. Moreover, *K* shows larger values in the radial than in the axial diffusion
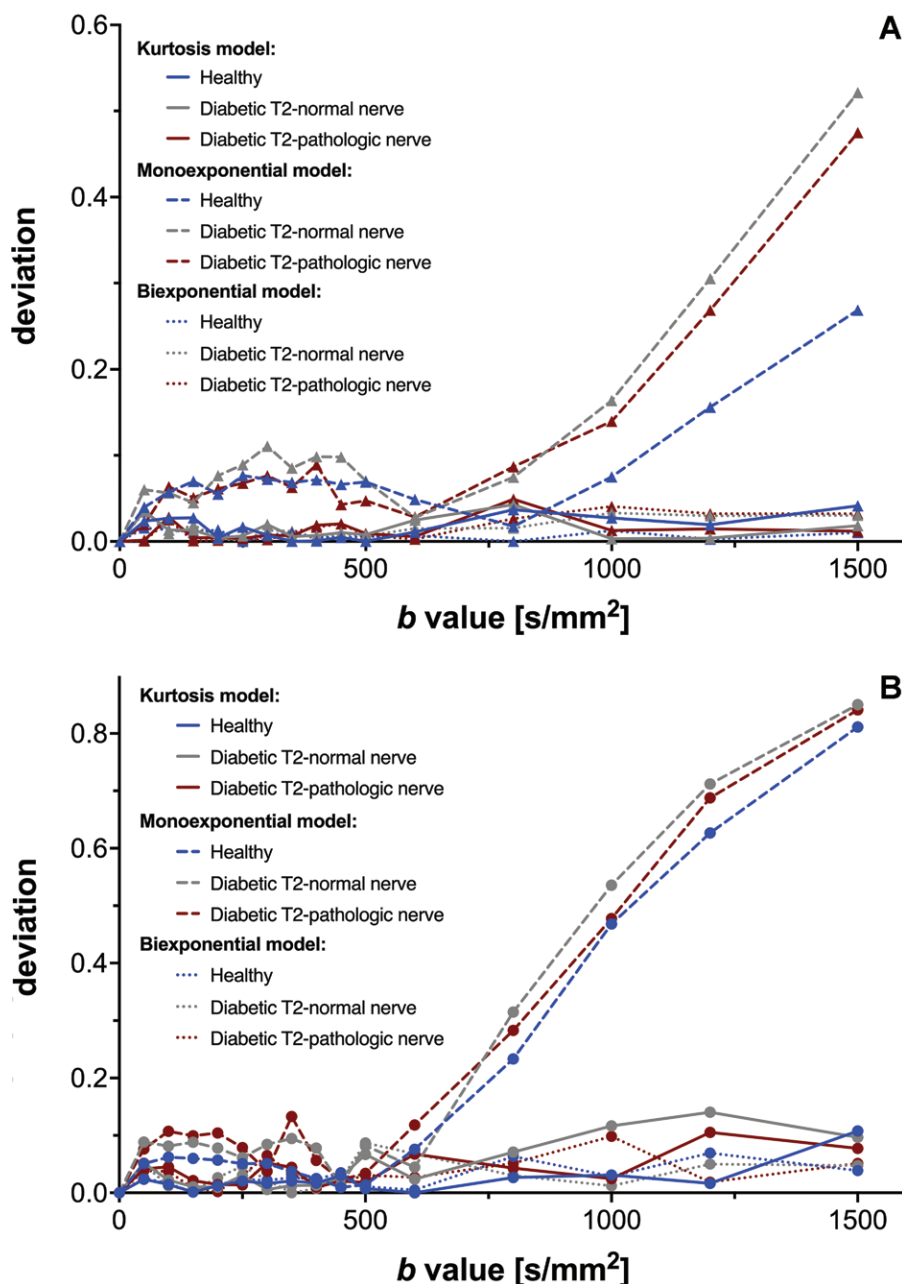
Figure 4: Goodness-of-fit assessment of the three models for healthy volunteers and participants with diabetes is shown as relative deviation of the individual model fits over the entire range of b values from the actual measurement values in **(A)** radial and **(B)** axial diffusion direction. At b values greater than approximately 800 sec/mm^2 and greater than approximately 600 sec/mm^2 in the radial and axial diffusion directions, respectively, monoexponential fitting does not provide a reasonable approximation of actually observed measurement values.

direction—at a consistently much higher SNR. This finding would be the other way round if only accounted for by an artificial noise floor effect.

Accordingly, extended diffusion models, namely the biexponential and kurtosis models, achieved a far better approximation of the measured nerve diffusion-weighted signal compared with standard monoexponential fitting, especially for b values over 600 sec/mm^2 in the axial and over 800 sec/mm^2 in the radial diffusion direction. Thus, our findings suggest an approximate optimal value of b of 700 sec/mm^2 for standard monoexponential DWI/DTI in the peripheral nervous system to achieve a high

degree of diffusion weighting and a high model accuracy. Still, the results presented herein must be interpreted with some caution due to numerous individual factors on a given MRI setup.

Kurtosis-derived metrics can provide unique information about nerve tissue microstructure as compared with conventional diffusion tensor estimates (24). In line with previous observations, K was higher in the radial than axial diffusion direction in our study, suggesting that the kurtosis excess is likely driven by fibers and axonal structures (21). Notably, K as well as D_k proved powerful in discriminating between healthy volunteers and participants with diabetes in the radial diffusional domain, even in
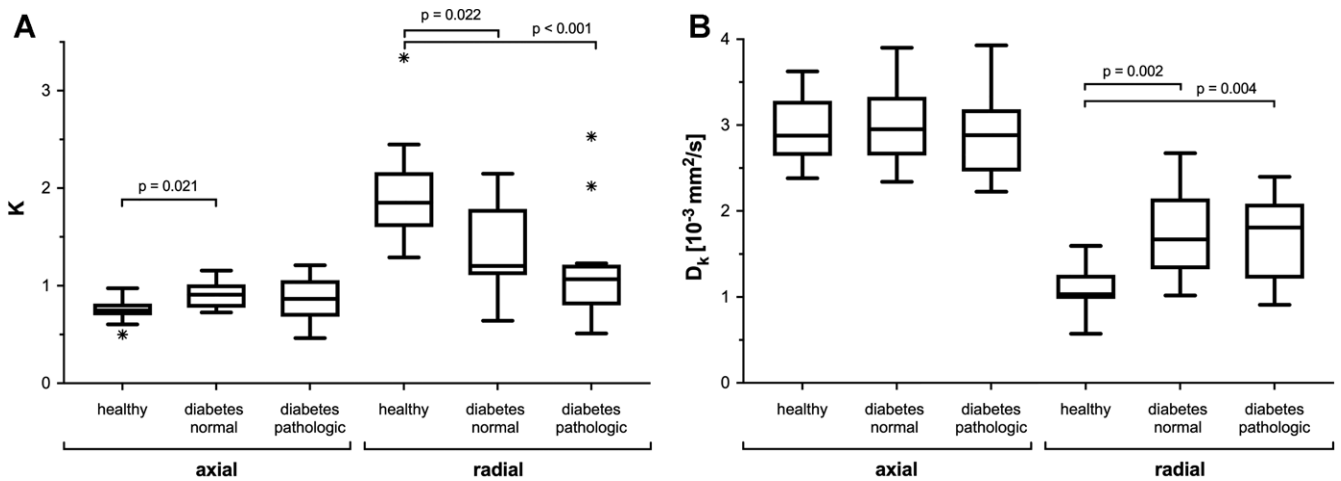
Figure 5: Box-and-whisker plots of the kurtosis parameters **(A)** K and **(B)** D_k for axial and radial diffusion directions in healthy volunteers and participants with diabetes. Significant group differences between healthy volunteers and participants with diabetes as well as between T2-normal and T2-pathologic nerve areas in participants with diabetes were found, especially in the radial diffusional domain. Data are medians (lines in boxes), 25th to 75th percentiles (bottom and top of boxes), and ranges (Tukey whiskers). Asterisks indicate outliers. P values were obtained with use of the Kruskal-Wallis test (healthy volunteers vs participants with diabetes) or Wilcoxon signed-rank test (T2-normal vs T2-pathologic nerve regions).
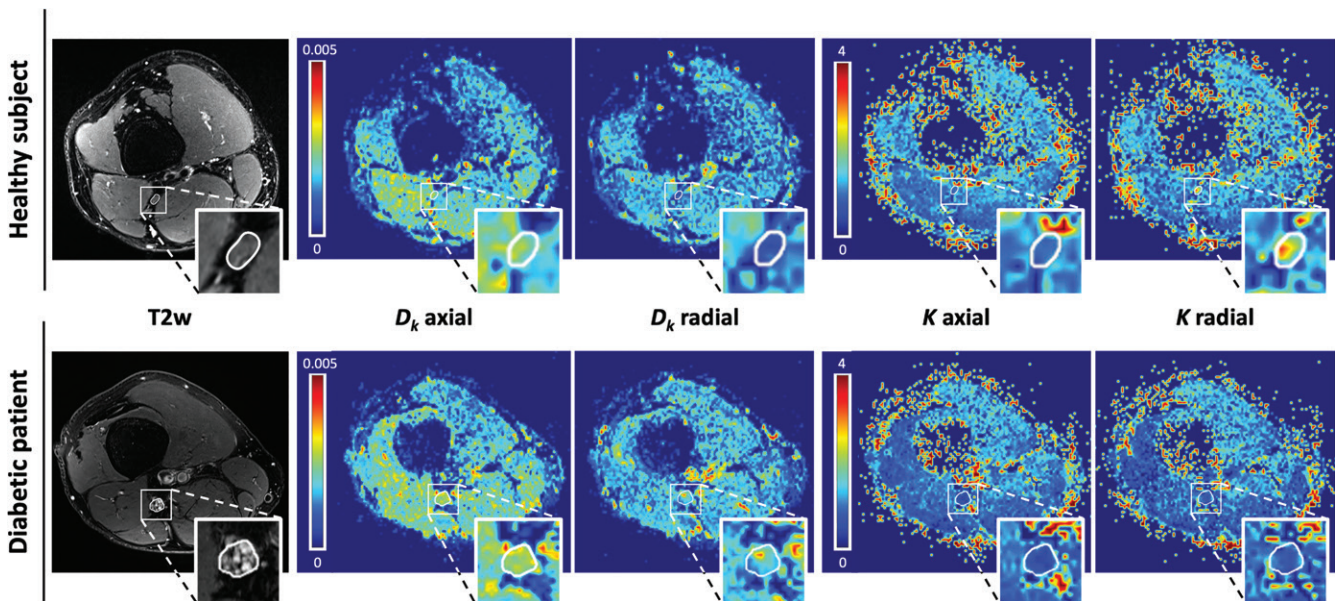
Figure 6: Representative T2-weighted (T2w) images of the distal sciatic nerve and corresponding color-coded parameter maps of D_k and K for axial and radial diffusion directions derived from the kurtosis model in a healthy volunteer (upper panel) and a patient with diabetes (participant 2 in Table 1) (lower panel). Segmentation of the tibial nerve portion is indicated by a white contour. Insets show magnification of the nerve. Compared with those in the healthy volunteer, higher D_k and lower K values can be seen in the participant with diabetes in the radial diffusional domain. D_k is in 10^{-3} mm²/sec.

apparently normal regions of the nerve at standard T2-weighted imaging, thereby possibly revealing pathophysiologic effects on nerve tissue microstructure that are missed at conventional T2-weighted imaging.

Interestingly, D_k does not seem to show a difference between healthy volunteers and participants with diabetes in the axial diffusion direction. This was unexpected, as healthy older individuals are believed to show a decrease in diffusion along the main axis of the nerve compared with younger controls (25); thus, this finding could represent a pseudo-normalization. Besides kurtosis-derived parameters, it is conceivable that an in-depth analysis of parameters derived from biexponential fitting

might contribute yet other new aspects of tissue microstructure that should be addressed in future studies.

A notable limitation of our study is that the two diffusion directions considered herein only represent approximations and were not defined retrospectively from multiple directions as done in DTI. It is also important to note that we used a multi–b-value experiment in which the pulse width as well as delta and echo time were kept constant while only the amplitude was varied. Further, the definition of normal and pathologic nerve regions in participants with diabetes was solely based on hyperintensities at T2-weighted MR neurography, thus potentially neglecting other nerve pathologies that would not manifest as a hyperintense lesion.

In summary, our study highlights the need for tissue-specific b value optimization in organs other than the central nervous system due to possible non-Gaussian diffusion behavior occurring already at low b values. We identify an optimal upper b value for reliable diffusion-weighted imaging/diffusion tensor imaging within peripheral nerves at approximately 700 sec/mm^2, providing a reasonable tradeoff between model accuracy and diffusion weighting. At higher b values, non-Gaussian models, such as kurtosis, may provide new insights into nerve pathophysiology.

References

1. Basser PJ, Mattiello J, LeBihan D. MR diffusion tensor spectroscopy and imaging. Biophys J 1994;66(1):259–267.
2. Xing D, Papadakis NG, Huang CL, Lee VM, Carpenter TA, Hall LD. Optimised diffusion-weighting for measurement of apparent diffusion coefficient (ADC) in human brain. Magn Reson Imaging 1997;15(7):771–784.
3. Subhawong TK, Jacobs MA, Fayad LM. Diffusion-weighted MR imaging for characterizing musculoskeletal lesions. RadioGraphics 2014;34(5):1163–1177.
4. Malayeri AA, El Khouli RH, Zaheer A, et al. Principles and applications of diffusion-weighted imaging in cancer detection, staging, and treatment follow-up. RadioGraphics 2011;31(6):1773–1791.
5. Partridge SC, Nissan N, Rahbar H, Kitsch AE, Sigmund EE. Diffusion-weighted breast MRI: clinical applications and emerging techniques. J Magn Reson Imaging 2017;45(2):337–355.
6. Hiltunen J, Suortti T, Arvela S, Seppä M, Joensuu R, Hari R. Diffusion tensor imaging and tractography of distal peripheral nerves at 3 T. Clin Neurophysiol 2005;116(10):2315–2323.
7. Kabakci N, Gürses B, Firat Z, et al. Diffusion tensor imaging and tractography of median nerve: normative diffusion values. AJR Am J Roentgenol 2007;189(4):923–927.
8. Kronlage M, Pitarokoili K, Schwarz D, et al. Diffusion tensor imaging in chronic inflammatory demyelinating polyneuropathy: diagnostic accuracy and correlation with electrophysiology. Invest Radiol 2017;52(11):701–707.
9. Bruno F, Arrigoni F, Mariani S, et al. Application of diffusion tensor imaging (DTI) and MR-tractography in the evaluation of peripheral nerve tumours: state of the art and review of the literature. Acta Biomed 2019;90(5-S):68–76.
10. Vaeggemose M, Pham M, Ringgaard S, et al. Magnetic resonance neurography visualizes abnormalities in sciatic and tibial nerves in patients with type 1 diabetes and neuropathy. Diabetes 2017;66(7):1779–1788.
11. Gasparotti R, Lodoli G, Meoded A, Carletti F, Garozzo D, Ferraresi S. Feasibility of diffusion tensor tractography of brachial plexus injuries at 1.5 T. Invest Radiol 2013;48(2):104–112.
12. Breckwoldt MO, Stock C, Xia A, et al. Diffusion tensor imaging adds diagnostic accuracy in magnetic resonance neurography. Invest Radiol 2015;50(8):498–504.
13. Jeon T, Fung MM, Koch KM, Tan ET, Sneag DB. Peripheral nerve diffusion tensor imaging: overview, pitfalls, and future directions. J Magn Reson Imaging 2018;47(5):1171–1189.
14. Le Bihan D. Apparent diffusion coefficient and beyond: what diffusion MR imaging can tell us about tissue structure. Radiology 2013;268(2):318–322.
15. Dietrich O, Heiland S, Sartor K. Noise correction for the exact determination of apparent diffusion coefficients at low SNR. Magn Reson Med 2001;45(3):448–453.
16. Jensen JH, Helpern JA, Ramani A, Lu H, Kaczynski K. Diffusional kurtosis imaging: the quantification of non-gaussian water diffusion by means of magnetic resonance imaging. Magn Reson Med 2005;53(6):1432–1440.
17. Veraart J, Poot DH, Van Hecke W, et al. More accurate estimation of diffusion tensor parameters using diffusion kurtosis imaging. Magn Reson Med 2011;65(1):138–145.
18. Le Bihan D. What can we see with IVIM MRI? Neuroimage 2019; 187:56–67.
19. Jensen JH, Helpern JA. MRI quantification of non-Gaussian water diffusion by kurtosis analysis. NMR Biomed 2010;23(7):698–710.
20. Pham M, Oikonomou D, Bäumer P, et al. Proximal neuropathic lesions in distal symmetric diabetic polyneuropathy: findings of high-resolution magnetic resonance neurography. Diabetes Care 2011;34(3):721–723.
21. Wu EX, Cheung MM. MR diffusion kurtosis imaging for neural tissue characterization. NMR Biomed 2010;23(7):836–848.
22. Andreisek G, White LM, Kassner A, Tomlinson G, Sussman MS. Diffusion tensor imaging and fiber tractography of the median nerve at 1.5T: optimization of b value. Skeletal Radiol 2009;38(1):51–59.
23. Guggenberger R, Eppenberger P, Markovic D, et al. MR neurography of the median nerve at 3.0T: optimization of diffusion tensor imaging and fiber tractography. Eur J Radiol 2012;81(7):e775–e782.
24. Hui ES, Cheung MM, Qi L, Wu EX. Towards better MR characterization of neural tissues using directional diffusion kurtosis analysis. Neuroimage 2008;42(1):122–134.
25. Kronlage M, Schwehr V, Schwarz D, et al. Peripheral nerve diffusion tensor imaging (DTI): normal values and demographic determinants in a cohort of 60 healthy individuals. Eur Radiol 2018;28(5):1801–1808.